

Impact of trailing wake drag on the statistical properties and dynamics of finite-sized particle in turbulence

Enrico Calzavarini^a, Romain Volk^a, Emmanuel Lévêque^a, Jean-François Pinton^a, Federico Toschi^b

^aLaboratoire de Physique, Ecole Normale Supérieure de Lyon, CNRS and Université de Lyon, 46 Allée d'Italie, 69007 Lyon, France.
International Collaboration for Turbulence Research

^bDept. Physics and Dept. Mathematics & Computer Science and J. M. Burgers Centre for Fluid Dynamics,
Eindhoven University of Technology, 5600 MB Eindhoven, The Netherlands.
International Collaboration for Turbulence Research.

arXiv:1008.2888v1 [physics.flu-dyn] 17 Aug 2010

Abstract

We study by means of an Eulerian-Lagrangian model the statistical properties of velocity and acceleration of a neutrally-buoyant finite-sized particle in a turbulent flow statistically homogeneous and isotropic. The particle equation of motion, beside added mass and steady Stokes drag, keeps into account the unsteady Stokes drag force - known as Basset-Boussinesq history force - and the non-Stokesian drag based on Schiller-Naumann parametrization, together with the finite-size Faxén corrections. We focus on the case of flow at low Taylor-Reynolds number, $Re_\lambda \simeq 31$, for which fully resolved numerical data which can be taken as a reference are available (Homann & Bec **651** 81-91 *J. Fluid Mech.* (2010)). Remarkably, we show that while drag forces have always minor effects on the acceleration statistics, their role is important on the velocity behavior. We propose also that the scaling relations for the particle velocity variance as a function of its size, which have been first detected in fully resolved simulations, does not originate from inertial-scale properties of the background turbulent flow but it is likely to arise from the non-Stokesian component of the drag produced by the wake behind the particle. Furthermore, by means of comparison with fully resolved simulations, we show that the Faxén correction to the added mass has a dominant role in the particle acceleration statistics even for particle with size in the inertial range.

Keywords: disperse multiphase flows, turbulence, Faxén, drag, history force

1. Introduction

The exact dynamics of a material particle in an inhomogeneous unsteady flow involves nonlinear equations that can be treated analytically only in approximate form^{1,2,3,4}. For this reason, several simplified models for the hydrodynamic forces acting on a particle have been proposed in the literature^{5,6}. It is still unclear however to what extent these models provide an accurate description in turbulent flow conditions, even in an averaged or statistical sense. A proper statistical description of particle dynamics would be a first important step towards building constitutive equations for the particulate phase carried by turbulent fluids. It would also be of practical importance for the many environmental phenomena and industrial applications in which particle suspensions in turbulence are involved. We intend here to contribute to this goal by carrying out refined simulations of particles in turbulent flow, and discriminate whether the particle model employed leads to physically sound results, in agreement with recent experiments and with fully resolved direct numerical simulations.

In previous studies, we have addressed the dynamics of small material particles with a description based on a minimal La-

grangian model accounting for pressure gradient, added mass term, and steady Stokes drag force^{7,8}. While this system produces several features of particle dynamics, like clustering and segregation as well as single-/multi-time statistics of acceleration and velocity, it fails to predict some statistical properties, particularly when the size of the particle is progressively increased above the dissipative scale of turbulence⁹. In order to better understand these discrepancies we have focused on the case of finite-sized and neutrally buoyant particles. We have proposed that Faxén corrections are the essential ingredients to account for the statistical properties of finite-sized particle acceleration in turbulence¹⁰. Numerical predictions of the particle acceleration variance (and of its probability density function) based on the Faxén argument were compared with experiments made in wind-tunnel¹¹ and resulted in agreement with Von Karman flow measurements¹². In a more recent work, experimental measurements support also other trends highlighted by the Faxén model: the effect of decrease of acceleration flatness as a function of the particle-size and the corresponding growth of the correlation time of the acceleration¹³.

Another series of numerical studies were recently conducted by Homann and Bec¹⁴ (HB in the following). These authors employed a direct numerical approach. They tracked the motion of a neutrally buoyant finite-sized particle in a turbulent flow by enforcing the no-slip velocity at the particle surface via a

*Corresponding authors:

Email addresses: ecalzavarini@gmail.com (Enrico Calzavarini),
romain.volk@ens-lyon.fr (Romain Volk)

penalty method on the discretized Navier-Stokes equation. In such a way they have been able to access the dynamics of a single finite-size particle in the diameter range $[2, 16]\eta$ in a moderately turbulent flow at $Re_\lambda = 32$. Both velocity and acceleration statistics were investigated. Therefore, HB measurements provides a set of reference data against which one can test particle Lagrangian models, as attempted here. The scope of this work however goes beyond the validation of a model equation. We aim also at having a physical picture of the statistical dynamics of particles. We have specific questions in mind: What is the statistical effect of the drag, particularly the trailing wake drag, on the dynamics of a neutrally-buoyant finite-size particle in turbulent flow? Does it modify the acceleration statistics or rather the velocity one? Is the role of Faxén correction still relevant for particles with size in the inertial range? We will see how our study provides an answer to these questions and a possible interpretation of the phenomenological picture.

The paper is organized as follow. In section 2 we describe the approach adopted in this study, we introduce the Lagrangian modeling of the particle dynamics, its numerical implementation, and some expected trends for the particle velocity and acceleration in the vanishing-size limit. In section 3 we present the results of the numerical study, starting from the particle Reynolds number behavior, and addressing then acceleration and velocity statistics as a function of the particle size. Comparison with direct numerical simulation data is discussed in detail in section 4. In the conclusions we summarize the main results and and give suggestions for possible future experimental/numerical investigations.

2. Methods

2.1. Particle equation of motion

We consider a Lagrangian equation of motion one-way coupled to a continuum flow $\mathbf{u} \equiv \mathbf{u}(\mathbf{x}, t)$. Such an equation keeps into account the pressure gradient and added mass term ($\sim D\mathbf{u}/Dt$), the drag force and the volume and surface Faxén corrections. The drag force is divided into three parts: the steady Stokes drag, the unsteady Stokes drag force or History force, and the non-Stokesian drag force. All together it reads as follow:

$$\frac{d\mathbf{v}}{dt} = \beta \left[\frac{D\mathbf{u}}{Dt} \right]_V + \frac{3\nu\beta}{r_p^2} ([\mathbf{u}]_S - \mathbf{v}) \quad (1)$$

$$+ \frac{3\beta}{r_p} \int_{t-t_h}^t \left(\frac{\nu}{\pi(t-\tau)} \right)^{\frac{1}{2}} \frac{d}{d\tau} ([\mathbf{u}]_S - \mathbf{v}) d\tau \quad (2)$$

$$+ c_{Re_p} \frac{3\nu\beta}{r_p^2} ([\mathbf{u}]_S - \mathbf{v}) \quad (3)$$

where r_p is the particle radius, ν the kinematic viscosity, β the density coefficient $\beta \equiv 3\rho_f/(\rho_f + 2\rho_p)$. Following² the Faxén corrections are expressed as volume and surface average of the

continuum fields $D\mathbf{u}/Dt$ and \mathbf{u} over a sphere of radius r_p centered at the particle position, respectively:

$$\left[\frac{D\mathbf{u}}{Dt} \right]_V = (4/3\pi r_p^3)^{-1} \int_V \frac{D\mathbf{u}}{Dt}(\mathbf{x}, t) d^3x \quad (4)$$

$$[\mathbf{u}]_S = (4\pi r_p^2)^{-1} \int_S \mathbf{u}(\mathbf{x}, t) d^2x \quad (5)$$

The history force is based here on the Basset-Boussinesq diffusive kernel, $\sim (t-\tau)^{-1/2}$, while t_h is the time over which the memory effect is significant. The non-Stokesian drag coefficient c_{Re_p} models the effect of the drag induced by the presence of a wake behind the particle. Of course in a Lagrangian model of particle dynamics, which is only one-way coupled to the fluid flow, no wake can be produced. Therefore, we resort to a model: The well known Schiller-Naumann (SN) parametrization¹⁵. The c_{Re_p} coefficient, which is a function of the particle-Reynolds number based on the diameter size $d_p \equiv 2r_p$ and on an estimator of the slip velocity, $Re_p \equiv |[\mathbf{u}]_S - \mathbf{v}|d_p/\nu$, is chosen to have the form $c_{Re_p} = 0.15 \cdot Re_p^{0.687}$ considered to be a good approximation whenever $Re_p < 1000$ ¹⁶. We note also that direct numerical simulations of the flow around a solid particle maintained fixed in a turbulent flow shows a good agreement between the real force acting on the particle (as computed from strain tensor at the surface of the particle) and the drag computed from the slip velocity with Schiller-Naumann parametrization^{17,18}.

2.2. Numerical implementation

We aim at studying the statistical signature of the different forces acting on the particle. For this reason in our numerical simulations we follow the trajectories of four species (or families) of particles with slightly different evolution equations. The first family is described by (1), it includes only the added-mass term and the steady Stokes drag and their Faxén corrections. It will be called Faxén model with Stokes drag. The second family is defined by (1)+(2), hence it includes also the history force. The third is based on (1)+(3), therefore the Schiller-Naumann correction is here included but not the history force. Finally the fourth family (1)+(2)+(3) keeps into account all the effects.

Particle type	Eq.
Faxén model with Stokes drag	(1)
+ History force	(1, 2)
+ Non-Stokesian drag	(1, 3)
+ Non-Stokesian drag + History force	(1, 2, 3)

Table 1: The four particle families considered in the present study and their respective equations of motion.

In total we integrate simultaneously the dynamics of $N_p = 1.28 \cdot 10^6$ particles. This ensemble is divided into 4 families, each family having 8 different sizes, in the diameter range $d_p \in [0, 32]\eta$. This amount to $3.2 \cdot 10^4$ particles per type.

2.2.1. Faxén Forces

The implementation of Faxén averages in our simulation is based on the Gaussian approximation proposed in a previous study¹⁰. The volume average of fluid acceleration at particle position is replaced by a local interpolation at the particle position of the continuum field after convolution by a three-dimensional Gaussian envelope $G(\mathbf{x})$, with unit volume and standard deviation σ . Convolutions are efficiently computed in spectral space, the volume averaged field hence reads:

$$\left[\frac{D\mathbf{u}}{Dt}(\mathbf{x}, t) \right]_V \approx \int_{L^3} G(\mathbf{x}') \frac{D\mathbf{u}}{Dt}(\mathbf{x} - \mathbf{x}', t) d^3x' \quad (6)$$

$$= \mathcal{DFT}^{-1} \left[\tilde{G}(\mathbf{k}) \frac{D\tilde{\mathbf{u}}}{Dt}(\mathbf{k}, t) \right] \quad (7)$$

where \mathcal{DFT}^{-1} denotes a discrete inverse Fourier transform on a cubic grid with N^3 nodes, while the over script \sim indicates a direct Fourier transform, $\tilde{G}(\mathbf{k}) = \exp(-\sigma^2 \mathbf{k}^2/2)$ being the Fourier transform of $G(\mathbf{x})$. We note that by setting the standard deviation $\sigma \equiv r_p/\sqrt{5}$, in the limit of small radii one gets $\tilde{G}(\mathbf{k}) \approx 1 - (r_p^2/10)\mathbf{k}^2 + \mathcal{O}(r_p^4)$ which leads to the correct first order Faxén correction in real space, i.e., $\mathbf{u} + (r_p^2/10)\Delta\mathbf{u} + \mathcal{O}(r_p^4)$. Analogously the surface average reads:

$$[\mathbf{u}(\mathbf{x}, t)]_S = \frac{1}{3r_p^2} \frac{d}{dr_p} \left(r_p^3 [\mathbf{u}(\mathbf{x}, t)]_V \right) \quad (8)$$

$$= \mathcal{DFT}^{-1} \left[\left(1 - \sigma^2 \mathbf{k}^2/3 \right) \tilde{G}(\mathbf{k}) \tilde{\mathbf{u}}(\mathbf{k}, t) \right]. \quad (9)$$

For clarity in Figure 1 the shape of the two convolution kernels (volume and surface) in real space are shown. The figure also shows for comparison the so called *optimal* convolution kernels, corresponding respectively to a three dimensional spherical gate function of volume $4/3\pi r_p^3$ for volume average and to a delta function over a spherical shell for surface average. Of course the implementation of such *optimal* averages in real space would be computationally more expensive. In section 4 we will investigate in detail the bias induced on the particle dynamics by the use of such a Gaussian approximation for Faxén corrections instead of the rigorous definition.

2.2.2. History Force

The Basset-Boussinesq history force can be computationally very expensive. This is due to the fact that the integral which is involved should be performed at each time-step on the full particle history. Furthermore the diffusive kernel, $\sim (t - \tau)^{-1/2}$ has a very slow decay and require a long memory time - virtually $t_h = \infty$ - to reach convergence. It is known however that the diffusive kernel overestimate the history force for particles characterized by finite Reynolds numbers Re_p ¹⁹. The formation of a trailing wake either stationary, unstationary or even turbulent is always associated to history kernel which decay faster than the Basset-Boussinesq²⁰. Equivalently we can say that in $Re_p \gg 1$ conditions the Basset-Boussinesq history force should have a shorter memory time windows t_h . This latter idea have been exploited in the computational approach called windows method²¹. Recently a more performant method based on the fit of the diffusive kernel tail via a series of exponential functions has also been proposed²². In this study we adopt a simple

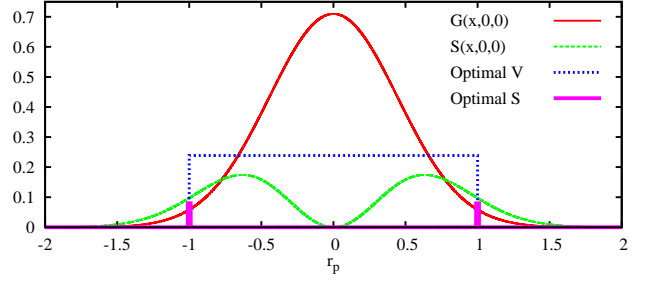


Figure 1: Real space one-dimensional projection, on the direction $(x,0,0)$, of filter functions. The volume gaussian filter is $G(\mathbf{x}) = (1/(\sqrt{2\pi}\sigma))^3 \exp(-\mathbf{x}^2/(2\sigma^2))$, while the surface convolution kernel turns out to be $S(\mathbf{x}) = (\mathbf{x}^2/(2\sigma^2))G(\mathbf{x})$. The optimal shape of volume and surface filter functions are also shown. The volume filter function is a three dimensional spherical gate function with total volume $4/3\pi r_p^3$, while the surface one is a delta function over the surface of the sphere but normalized in such a way that its volume integral is $4\pi r_p^2$.

windows approximation: instead of setting $t_h = \infty$ we chose $t_h \approx 10\tau_\eta$ but keep the diffusive kernel functional form. This choice is based on the observation that in the turbulent conditions considered in our study after a time $10\tau_\eta$ the Lagrangian signal $d([\mathbf{u}]_S - \mathbf{v})/dt$ is already completely uncorrelated. The short memory on the history force is therefore not given by the specific kernel form (which is indeed almost flat in our case) but from the relatively short correlation time of the turbulent flow. With this choice, t_h corresponds approximately to 10^3 time-steps of our simulations, which are stored and used for the discrete estimation of the history integral at each time-step. We note that our t_h satisfy the criterion given in ref.^{21,6} for the windows method and it has a double extension in time steps respect to the time windows considered in the numerical validations considered in ref.²². We have also performed a *posteriori* check in which the pre-recorded $d([\mathbf{u}]_S - \mathbf{v})/dt$ signal has been used to compute the history force with different values of the windows length. This test has further confirmed the convergence and reliability of the adopted implementation.

2.2.3. Eulerian dynamics

A suitable turbulent flow is generated by integrating the Navier-Stokes equation in a cubic box of size $L = 2\pi$ with periodic boundary conditions. The flow is forced on the largest shells in spectral space, on the wave-vectors for which the condition $\mathbf{k}^2 \leq 2^2(2\pi L)^2$ is satisfied. The force we adopt in this study keeps fixed the amplitude of kinetic energy of the large scales. More details concerning the values of relevant input and output quantities of the numerical simulation of this turbulent flow are provided in Table 2.

2.3. Faxén corrections and small particle limit predictions

In the study of Homann and Bec¹⁴ a derivation of the functional behavior of the variance of particle velocity and acceleration in the limit of vanishing particle diameters d_p has been proposed. The argument is based on a perturbative expansion

of the Faxén correction for the velocity. This reads as ¹:

$$\mathbf{v} \simeq [\mathbf{u}]_S \simeq \mathbf{u} + \frac{d_p^2}{24} \Delta \mathbf{u} + O(d_p^4). \quad (10)$$

Furthermore, the hypothesis of a spatially homogeneous particle distribution in the limit $d_p \rightarrow 0$ is made. By squaring Eqn. (10), retaining only quadratic terms in d_p , and averaging over the particle ensemble and in time, $\langle \dots \rangle$, one gets:

$$\langle \mathbf{v}^2 \rangle \simeq \langle \mathbf{u}^2 \rangle - \frac{d_p^2}{12} \langle \mathbf{u} \Delta \mathbf{u} \rangle = \langle \mathbf{u}^2 \rangle - \frac{d_p^2}{12} \frac{\varepsilon}{\nu} = \langle \mathbf{u}^2 \rangle - \frac{5}{3} \left(\frac{d_p}{2\lambda} \right)^2, \quad (11)$$

where $\varepsilon \equiv (\nu/2) \langle (\nabla \mathbf{u} + (\nabla \mathbf{u})^T)^2 \rangle = \nu L^{-3} \int_{L^3} \mathbf{u} \Delta \mathbf{u} \, d^3x$ is the mean energy dissipation rate and $\lambda \equiv (5\nu \langle \mathbf{u}^2 \rangle / \varepsilon)^{1/2}$ is the Taylor micro-scale. If we instead (i) derive with respect to time Eqn. (10), (ii) make the assumption $D/Dt \simeq d/dt$, and then (iii) square and average the result, we obtain an approximate prediction for the acceleration variance

$$\langle \mathbf{a}^2 \rangle \simeq \left\langle \left(\frac{D\mathbf{u}}{Dt} \right)^2 \right\rangle - \frac{d_p^2}{12} \left\langle \left\| \frac{D(\nabla \mathbf{u})}{Dt} \right\|^2 \right\rangle. \quad (12)$$

We will see in the following to which extent these approximations can be considered appropriate to describe the particle behavior. We note that in the simulations we have direct access to the values $\langle ([\mathbf{u}]_S)^2 \rangle$ and $\langle ([D\mathbf{u}/Dt]_V)^2 \rangle$ which can be used for comparison. Finally, it is also worth noting that the particle Reynolds number Re_p is proportional to $|\mathbf{v} - [\mathbf{u}]_S|$, this means that in the small-particle limit the leading order is $O(d_p^4)$, hence one expects $Re_p \sim d_p^5$.

3. Results

3.1. Particle Reynolds number

We begin investigating the particle Reynolds number Re_p as a function of the particle diameter, with measurements reported in Fig. 2. First we note that in the range $d_p \in [3.2, 32]\eta$ the mean Reynolds number varies considerably, three order of magnitudes from 10^{-1} to about 10^2 . We can immediately observe that the particle models which are making use only of Stokes drag forces - that is to say based on the assumption $Re_p < 1$ - can not be considered entirely consistent. Such models underestimate the actual drag on the particle. This is clearly noticeable for the Faxén model with Stokes drag in the large- d_p range, when Re_p attains the maximal value $\mathbf{u}_{rms} d_p / \nu$, corresponding to a ballistic particle velocity \mathbf{v} not varying in time and not correlated to the local fluid velocity $[\mathbf{u}]_S$. We note instead that for all the models in the small particle limit we have a steeper scaling (slope 4.50 ± 0.05), close to the expected d_p^5 . Hence, in the small particle regime \mathbf{v} and $[\mathbf{u}]_S$ are highly correlated, differing only by $O(d_p^4)$ terms. We also notice that, while the history force produces just a shift, the non-Stokesian drag term changes the slope in the large particle regime. This apparently minimal variations have, as we will see later on, important consequences on the statistics of the particle velocity variance.

¹Note that (10) corrects a typo contained in ref. ¹⁴ on the numerical coefficient in front of $d_p^2 \Delta \mathbf{u}$, which had affected all the predictions proposed in that study. Our calculations for eq. (11) provides a coefficient 5/3, instead of 1/100 given in ¹⁴. Furthermore in eq. (12) we find the coefficient 1/12, and not 1/20.

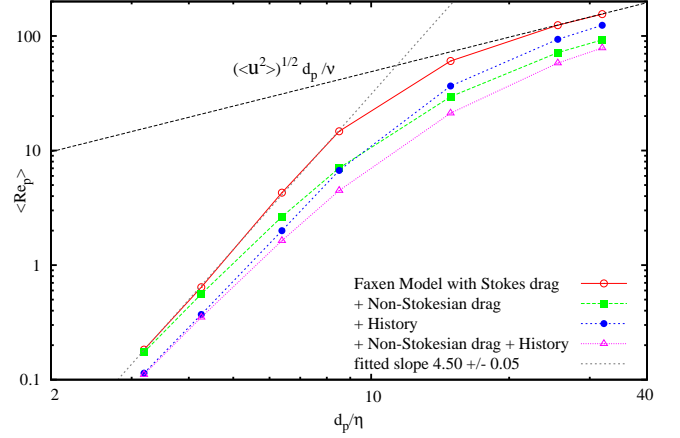


Figure 2: Mean particle Reynolds number, $\langle Re_p \rangle$, versus the diameter in Kolmogorov scale units, d_p/η , from the four different models. A power-law fit to the Faxén model with Stokes drag on the smallest particle sizes is shown, we get a 4.5 slope. For the same model, the maximal Reynolds number $\mathbf{u}_{rms} d_p / \nu$ is reached by the largest particles.

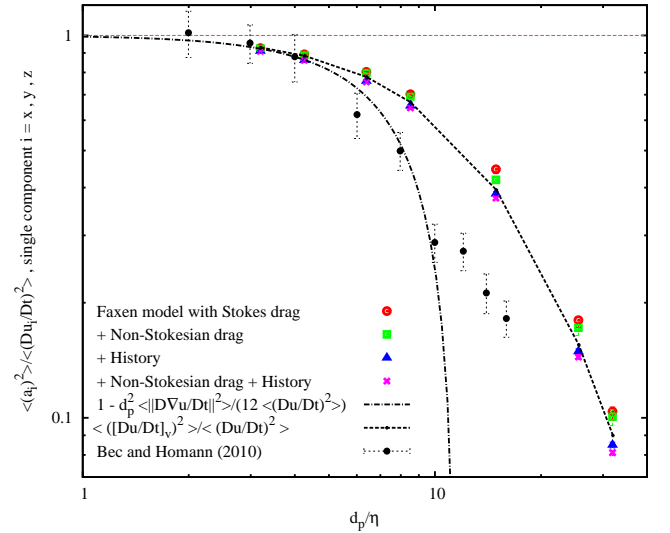


Figure 3: Normalized single-component particle acceleration variance for particles of different sizes: $\langle (a_i)^2 \rangle / \langle (D_t u_i)^2 \rangle$ vs. d_p/η . Here $\langle (D_t u_i)^2 \rangle$ is the fluid tracer acceleration variance or equivalently the Eulerian acceleration averaged over time and space. The behavior of the four different models adopted is reported. The dashed-dotted line represent the behavior of particle acceleration variance expected to originate from Faxén corrections in the small particle limit (see eq (12)). The dotted line represents the ratio of the variance of the volume filtered eulerian field $[D\mathbf{u}/Dt]_V$ to the fluid acceleration variance.

N^3	δx	δt	ν	ε	η	τ_η	u_{rms}	λ	T_E	L_E	Re_λ	t_{tot}
128 ³	$4.9 \cdot 10^{-2}$	$3.2 \cdot 10^{-3}$	$4.4 \cdot 10^{-2}$	$7.5 \cdot 10^{-1}$	$1.0 \cdot 10^{-1}$	$2.4 \cdot 10^{-1}$	1.2	1.1	2.9	3.5	31	192

Table 2: Parameters of the numerical simulation: N number of grid points per spatial direction; $\delta x = 2\pi/N$ and δt are the spatial and temporal discretization; ν is the value of kinematic viscosity; ε the mean value of the energy dissipation rate. $\eta = (\nu^3/\varepsilon)^{1/4}$ and $\tau_\eta = (\nu/\varepsilon)^{1/2}$ are the Kolmogorov dissipative spatial and temporal scales, $u_{rms} = (\overline{u_i u_i})_V/3)^{1/2}$ the single-component root-mean-square velocity, $\lambda = (15 \nu u_{rms}^2/\varepsilon)^{1/2}$ the Taylor micro-scale, $T_E = (3/2)u_{rms}^2/\varepsilon$ and $L_E = u_{rms} T_E$ are the Eulerian large-eddy-turnover temporal and spatial scales; $Re_\lambda = u_{rms} \lambda/\nu$ the Taylor scale based Reynolds number. t_{tot} is the total simulation time in statistically stationary conditions and the total time-span of particle trajectories.

3.2. Acceleration statistics

We examine now some statistical properties of the acceleration. In Figure 3 we show the behavior of the single-component particle acceleration variance $\langle a_i^2 \rangle$ normalized by the fluid acceleration variance $\langle (D_t u_i)^2 \rangle$ as a function of the particle size in d_p/η units. It is remarkable to note that all the particle models leads to very similar results. The History force or the Non-Stokesian drag have no effect, at least for this observable. The overall trend of the acceleration variance is dominated by the Faxén Volume correction, $\langle a_i^2 \rangle \simeq \langle [D\mathbf{u}_i/Dt]_V^2 \rangle$ with $[D\mathbf{u}_i/Dt]_V$ sampled homogeneously in space over the field (see Fig. 3). Equation (12) based on the first order approximation, although qualitatively correct, fails to predict quantitatively the measurements for $d_p > 4\eta$. In Figure 3 we have plotted the data points from HB¹⁴. The agreement with our data is excellent up to $d_p \simeq 4\eta$, while the Lagrangian model shows a less pronounced decrease (approximately by a factor of two) for larger diameters. We will analyze the possible origin of these difference in section 4.

In Figure 4 we show the measurements of the acceleration flatness $F(a_i) = \langle a_i^4 \rangle / (\langle a_i^2 \rangle)^2$ normalized by the fluid acceleration flatness $F(D\mathbf{u}_i/Dt)$ versus particle size. As already noticed in¹⁰, and experimentally verified in¹³ the flatness decreases with increasing the particle size. Here the different Lagrangian models lead only to small shifts in the flatness value, hence the picture remains the same as for the variance. Although, HB direct numerical simulations may suffers of lack convergence the case of flatness, the measurements are in qualitative agreement with our simulations. Finally we look at the correlation time of the particle acceleration. As done before¹⁰, we define the acceleration correlation time as the integral of the correlation function from time zero till its first change of sign:

$$T_{a,p} = \int_0^{\tau_0} C_{a_i}(\tau) d\tau; \quad C_{a_i}(\tau) \equiv \frac{\langle a_i(t+\tau)a_i(t) \rangle}{\langle (a_i(t))^2 \rangle} \quad (13)$$

where $C_{a_i}(\tau_0) = 0$. We observe that, as soon as the particle size grows, the acceleration correlation time $T_{a,p}$ deviates from the tracer value $T_{a,f} (\simeq 1.2 \tau_\eta)$, Fig. 5. This growth, is a result of the Faxén averaging (in fact it is absent when averaging is not included, see the discussion in¹⁰) and comes from the fact that in finite-sized particles Stokes drag becomes negligible, leading to $d\mathbf{v}/dt \simeq [D\mathbf{u}/Dt]_V$. We note however that there is also a significant difference between the basic Faxén Stokes drag model, for which the mechanism explained before is at work, and the model with non-Stokesian drag, the latter one producing more correlation. This feature is rather surprising

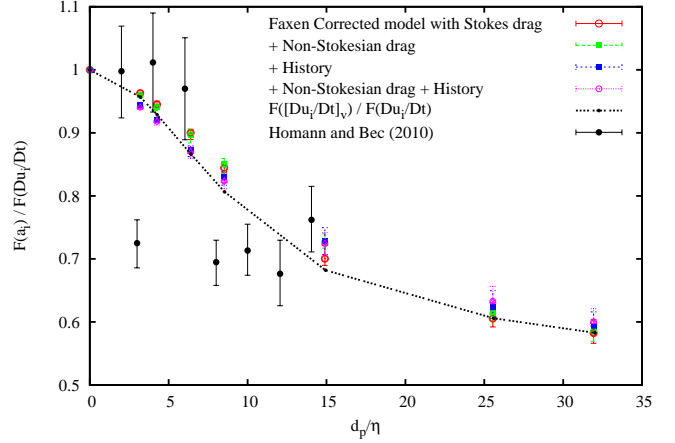


Figure 4: Single-component particle acceleration flatness, $F(a_i)$, normalized by the fluid tracer acceleration flatness, $F(D\mathbf{u}_i)$, as a function of the flatness of the particle diameter in η units. The dotted line represents the ratio of the flatness of the volume filtered eulerian field $[D\mathbf{u}/Dt]_V$ to the fluid acceleration flatness.

and has a different origin. One may think that including non-Stokesian drag, the effective response time of the particle, i.e., $1/\tau_{eff} = (1 + C_{Re_p})3\nu\beta/r_p^2$ is reduced, therefore the acceleration should be correlated on a shorter time scale $\sim \tau_{eff}$. As we will see later in section 3.3 when non-Stokesian drag is active, the drag is never negligible and $\mathbf{v} \simeq [\mathbf{u}]_S$, hence for the acceleration $d\mathbf{v}/dt \simeq d[\mathbf{u}]_S/dt$. It is clear that $d[\mathbf{u}]_S/dt = \partial_t [\mathbf{u}]_S + [\mathbf{u}]_S \cdot \partial [\mathbf{u}]_S$ does not have the sub-grid (sub particle-size) correlations included in $[D\mathbf{u}/Dt]_V = \partial_t [\mathbf{u}]_V + [\mathbf{u} \cdot \partial \mathbf{u}]_V$, which are correlated on shorter timescales.

Any Lagrangian model equation seems however to underestimate the real $T_{a,p}$ resulting from the HB direct numerical simulations. This fact has been also noticed, in a comparison of Faxén Lagrangian model with experimental data¹³.

3.3. Velocity statistics

Contrary to the acceleration's case the velocity particle statistics is deeply affected by the form of the particle dynamical equation. In Figure 6 we show as a function of the particle size the measurements of the deviation of normalized single-component particle velocity variance with respect to the velocity variance of the turbulent flow: $(\langle \mathbf{u}_i^2 \rangle - \langle \mathbf{v}_i^2 \rangle) / \langle \mathbf{u}_i^2 \rangle$. The first model - based simply on Faxén terms and Stokes drag - predicts for this quantity a non-monotonous behavior, leading for the bigger particle sizes to a velocity variance even larger than the fluid one. This results is rather unphysical (as it is

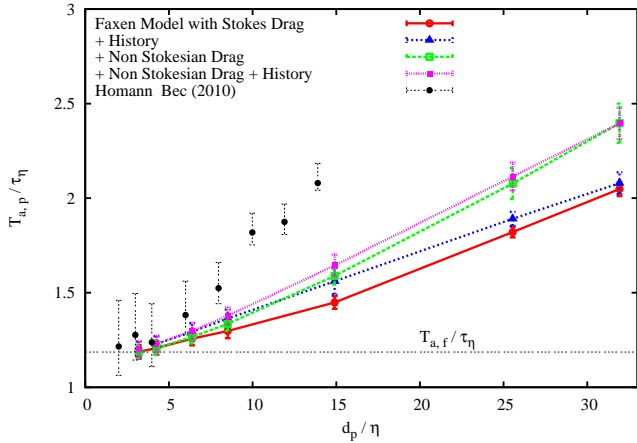


Figure 5: Correlation time of acceleration $T_{a,p}$, in τ_η units, as a function of the normalized particle diameter d_p/η .

not possible for a particle to be on average more energetic than the flow by which it is driven and transported) and clearly it represents a limitation of the basic Faxén model with Stokes drag. This limitation is readily cured whenever an extra drag force is added. Among History and non-Stokesian drag it is definitely the latter one bringing the most significant changes. The non-Stokesian drag reduces the kinetic energy of the particle as compared to the one of a fluid tracer, this energy decreases monotonically with the particle size. For comparison, in Figure 6 we have also reported the prediction in the limit of small-particles, eq. (11). As for the acceleration, this analytical prediction seems to be a good approximation to the measurements up to $d_p \simeq 4\eta$. We also report in Figure 6 the value of the variance of the Eulerian filtered field $[\mathbf{u}]_S$. One can note that by adding more drag to the basic Stokes term, the particle velocity approaches the filtered fluid velocity variance, i.e. $\mathbf{v} \rightarrow [\mathbf{u}]_S$. We note that the prediction of the Lagrangian models keeping into account all the considered effects eqs. (1)-(3), agree well with the HB data. Apart from the parabolic ($\sim d_p^2$) behavior for vanishing particle sizes no clear scaling of the normalized velocity variance can be detected from our measurement. In HB it was proposed that a scaling regime with slope $d_p^{2/3}$ would appear out of the Faxén dominated regime. This was attributed to the effect of the background turbulent flow, via the assumption $\langle v_i^2 \rangle \sim \langle (\delta u_d)^2 \rangle \sim d_p^{2/3}$ where the Kolmogorov scaling relation for the second order eulerian structure function $\langle (\delta u_r)^2 \rangle \equiv \langle (\mathbf{u}(\mathbf{x} + \mathbf{r}) - \mathbf{u}(\mathbf{x})) \cdot \hat{\mathbf{r}}^2 \rangle \sim r^{2/3}$ is implied. Here we would like to advance another explanation, the different scaling in that intermediate regime seems to be an effect of the drag term and in particular of the non-Stokesian drag (see again Figure 6). We note that non-Stokesian drag term included in our model equations based on SN parametrization accounts rather for the effect of a stationary wake behind the particle than for wake generated turbulent fluctuations. Given the good agreement of our data with HB measurements, our guess is that the background turbulent fluctuations plays only a minor role in determining the particle velocity statistics.

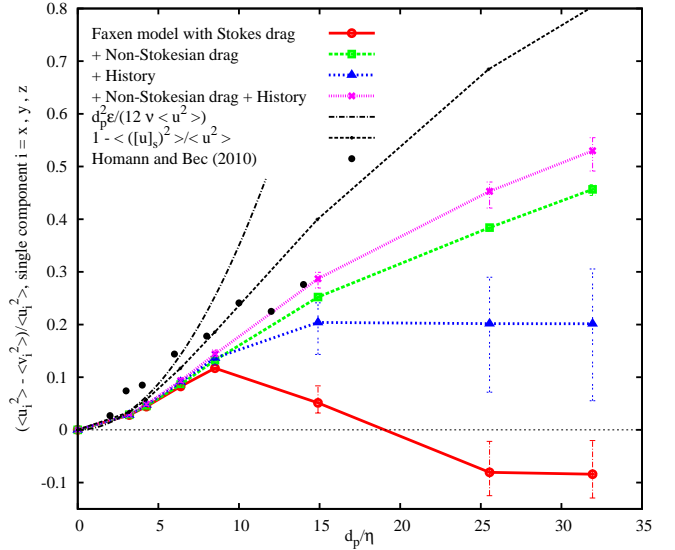


Figure 6: Deviation of the particle velocity variance from the fluid value, as a function of the dimensionless particle diameter d_p/η . The behavior of the four different models adopted is reported. The dashed-dotted line represent the deviation from the fluid root-mean-square (r.m.s.) velocity that is expected to originate from Faxén corrections in the small particle limit (see eq (11)). The dashed line represents the deviation of the variance of the surface filtered eulerian field $[\mathbf{u}]_S$ from the unfiltered velocity variance.

The non-Stokesian term has also important consequences on the velocity correlation time. Such a time can be defined as the time integral of the correlation function:

$$T_p = \int_0^{+\infty} C_{v_i}(\tau) d\tau; \quad C_{v_i}(\tau) \equiv \frac{\langle v_i(t+\tau)v_i(t) \rangle}{\langle (v_i(t))^2 \rangle} \quad (14)$$

As we have already mentioned, the Stokes drag force alone is not effective in slowing down the velocity especially for large particles. This produces quasi-ballistic trajectories, governed by $\mathbf{v}(t) \simeq \int_0^t [D_t \mathbf{u}(t')]_V dt'$, that tend to have very large correlation time. The non-Stokesian (or wake) drag provides instead a way to reduce particle speed, $\mathbf{v}(t) \simeq [\mathbf{u}]_S$ and its correlation time. This is evident from Figure 7 where the correlation functions for different terms for a large Stokesian and a large non-Stokesian particle are compared.

On Figure 8 the trend of the velocity correlation time as a function of the particle size is shown. Non-Stokesian drag produces a reduction of T_p of more than 100% as compared to the purely Stokesian case.

4. Discussion

In previous sections we have shown that the agreement of the Lagrangian model, even in its complete form eqs. (1),(2),(3), with the measurements from HB direct numerical simulations is rather satisfactory for the variance of the velocity as a function of the particle size. However, we observe systematic deviations when acceleration is concerned. Here we would like to discuss the causes of these discrepancies more in detail. We

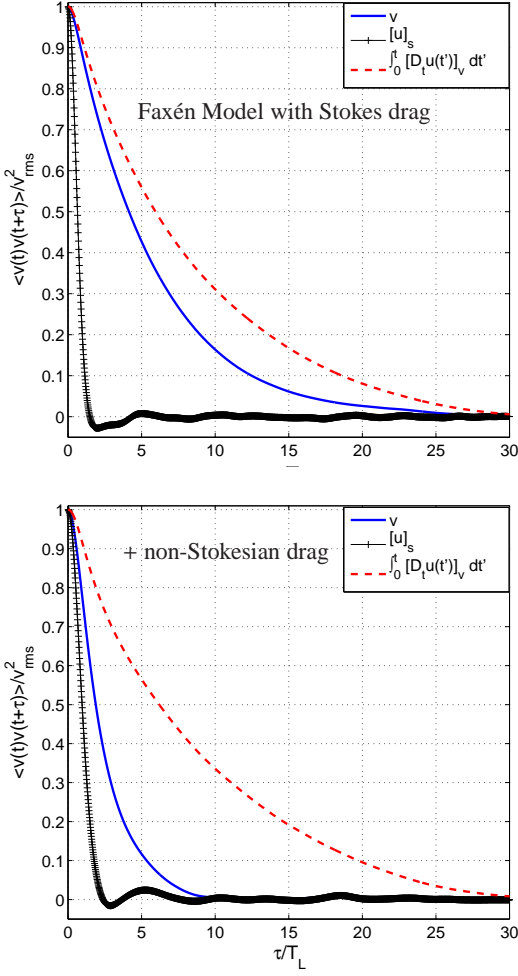


Figure 7: Correlation function of particle velocity \mathbf{v} , of the filtered fluid velocity along the particle trajectory $[\mathbf{u}]_s$, and of the time integral of fluid acceleration $\int_0^t [D_t \mathbf{u}(t')]_V dt'$ for particle size $d_p = 32\eta$. Faxén model with Stokes drag (top), with non-Stokesian drag (bottom).

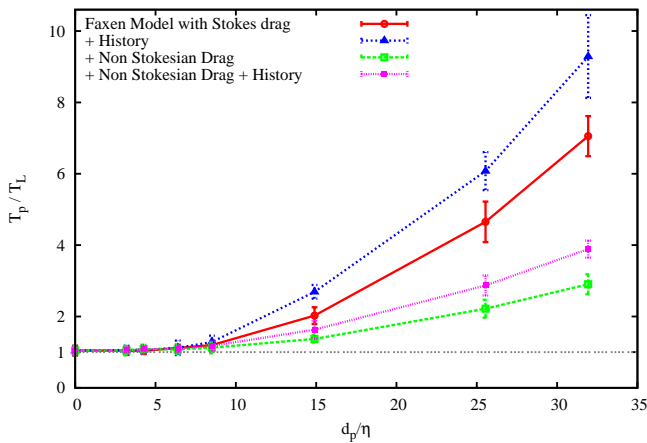


Figure 8: Integral correlation time of particle velocity T_p as a function of the diameter d_p . T_p is made dimensionless by the integral velocity correlation time of a Lagrangian tracer T_L , while the diameter is normalized by the dissipative scale η .

can advance the following hypothesis:

i) The differences originate from a limitation of the model which takes into account volume and surface averages only in the approximate form of a Gaussian convolution. Although this approximation is well tuned for the first order Faxén correction, it might be less accurate for larger particles, when roughly $d_p > 4\eta$.

ii) The model neglect the effect of particle interaction with its own wake. This effect, while negligible in a flow with a large mean component, might become relevant in the isotropic flow conditions considered here (and in HB work) where a particle can cross a region previously perturbed by its own wake.

iii) The observed discrepancies may come from differences in the simulated turbulent flows - in fact differences in the forcing at such small Reynolds number $Re_\lambda \sim 32$ may have consequences even on the small scale statistics. The point i) can be investigated carefully. In order to see if there is any bias induced by Gaussian averaging as compared to the mean over a sphere, we have averaged the a field $D\mathbf{u}(\mathbf{x}, t)/Dt$ over a large number of spheres of diameters d_p , uniformly distributed over random locations in space. This procedure is repeated over 250 Eulerian $D\mathbf{u}/Dt$ snapshots, equally spaced in time over an interval of $20 T_E$. Although this method is not precise for small sphere diameters when only few points of the discretized $D\mathbf{u}/Dt$ field enter into the average, for large diameters the average converges rapidly to the correct (continuum-limit) values. In figure 9 we report the results of these measurements for the variance and the flatness of $[D\mathbf{u}/Dt]_V(\text{sphere})$, as a function of d_p and we compare it with the Gaussian averages $[D\mathbf{u}/Dt]_V(\text{Gauss})$, and with the measurements on the Lagrangian models and DNS data. The result shows that the sphere average is sensibly different from the Gaussian convolution. For small particles the discretization bias fails to match the analytical prediction (11), which is instead well captured by the Gaussian distribution. For larger particle sizes the sphere average shows a stronger decrease of the variance as compared to the Gaussian case. Remarkably in this region the average over spheres agrees with the HB results. A similar scenario appears for the flatness fig. 9 (bottom). This finding is important at least for two reasons. First it shows that the Faxén correction to the fluid acceleration plays a central role in the particle acceleration statistics not only for a particle in the upper dissipative range $d_p < 4\eta$ but also for a particle with size is in the inertial range $d_p \leq 32\eta$. Second, it shows that, although the Gaussian convolution approximation is an efficient method to solve particle dynamics, it has limitations which becomes important approximately when $d_p > 4\eta$. The above observations have also an impact on the time-statistics: since a reduction of the variance of the filtered acceleration is associated to a slower fluctuations in time, we expect the correlation time of acceleration to increase for finite-sized particles. Hence the picture in fig 5 would change, solving the observed mismatch towards HB simulations and experiments¹³. However, this latter point may find a confirmations only in further studies.

Evaluating the impact of point ii) is unfortunately not possible in the framework of the present model. One would need to introduce a coupling (so called two-way coupling) between the

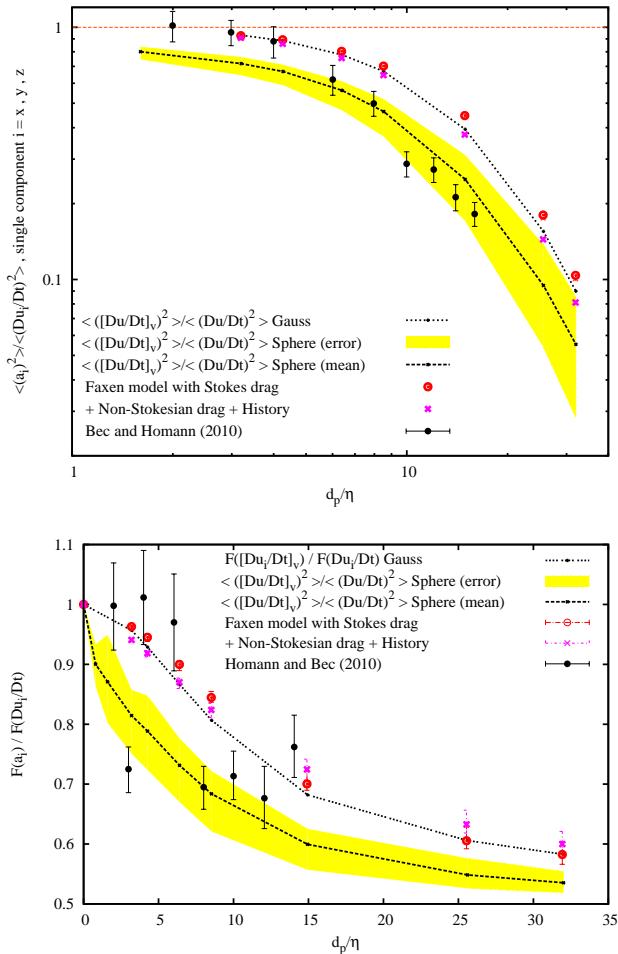


Figure 9: Comparison between acceleration variance (top panel) and flatness (bottom panel) We show data coming from Gaussian convolutions, same as in fig. 3, of the fluid acceleration field Du/Dt (dotted line), the quantity has been computed run-time therefore statistical errors are in this case of the order of the line thickness. Averages over spherical volumes (dashed line) are affected by a larger statistical uncertainty (yellow shaded region) which comes from the differences in the measurements between the three cartesian components. Measurements from the Lagrangian model based on eq (1) and eq. (1),(2),(3) are reported, together with HB data.

particle and the fluid enforcing conservation of the total momentum.

Finally on point iii), for completeness we shall note that there are some differences between the turbulent flows simulated by Homann & Bec and the one used here. While we adopt a forcing which keeps constant the energy on the largest Fourier modes (amplitude-driving), HB also uses a random forcing of the phase in Fourier space (phase-driving). While these differences have no effect in fully developed turbulent flows, at the small Reynolds number considered here, $Re_\lambda \simeq 32$, they might have an impact. We see indeed that while we find $\langle a_i^2 \rangle \varepsilon^{-3/2} \nu^{1/2} = 1.1$, $F(a_i) = 5.7$, Homann & Bec report $\langle a_i^2 \rangle \varepsilon^{-3/2} \nu^{1/2} = 1.3$ and $F(a_i) = 8.4$, hence a flow slightly more intermittent at small-scales. This prevents us, for instance, from a direct comparison on the shape of the probability density

functions of acceleration and velocity.

5. Conclusions

In this study we have focused on the statistical properties of acceleration and velocity of finite-sized neutrally-buoyant particles driven in a moderately turbulent homogeneous and isotropic flow. We have adopted a Lagrangian model particle equation which keeps into account inertia effect, size effects, and the drag forces resulting both from a Stokes flow around the particle and form an asymmetric trailing wake state via Schiller-Naumann modeling. We have studied the contribution of these forces separately, in particular the drag force has been divided into three components: Stokes, History, and non-Stokesian force.

We find that the drag forces have minor effect on the statistical properties of acceleration. Acceleration statistics seems to be dominated by inertia effect and by the Faxén corrections, whose influences extends also over particle with size in the inertial turbulent range.

On the opposite drag forces have important effects on the time integral of the acceleration, that is to say on the velocity statistics. This is particularly evident when considering the trend of the second order statistical moment (the variance) as a function of the particle size. For the case of neutrally buoyant particle analyzed here, the variance of the particle velocity from the different Lagrangian models start to separate at $d_p > 8\eta$, corresponding to a particle Reynolds number $Re_p \sim O(10)$. Above this threshold History and non-Stokesian drag have a dominant role. This lead us to propose that the trend observed for the particle velocity variance as a function of its size does not originate from inertial-scale properties of the background turbulent flow but arise from the non-Stokesian component of the drag produced by the wake behind the particle.

The effects detected in the velocity statistics are relevant for studies of particle dispersion in turbulence. For instance a simple finite-size particle model based on Stokes drag or history force only, would overestimate the average particle dispersion from a fixed source in space, and similarly for pair separation. Therefore, this study suggests that in order to validate Lagrangian models one should look not only into the small scale acceleration statistics - as done up to now in many studies - but also into velocity and possibly dispersion and pair separation statistics.

On the numerical side, we have shown that the Gaussian convolution approximation, despite its computational efficiency is not accurate when particles much larger than 4η are involved. On the other hand spherical averages in real space, as the one performed in our test, would be computationally very expensive and not enough accurate for small size particles (in particular it is not possible to capture the laplacian correction (10) when only few grid points are used). Future numerical studies should find a trade off between efficient computations and accuracy. A possible way, which however needs careful scrutiny and tuning, is to consider the implementation of convolution kernel functions with sharper boundaries. Furthermore, the effect of

two-way coupling in this type of homogeneous and isotropic turbulent flow deserve to be studied.

Acknowledgments: The authors are thankful to A. Naso and M. Bourgoïn for useful discussions. Support from COST Action MP0806 “Particles in turbulence”, from ANR-BLAN-07-1-192604 is acknowledged. E.C. was partially supported by the HPC-Europa2 visiting program. Numerics for this study have been performed at SARA (The Netherlands), CINECA (Bologna, Italy) and CASPUR (Roma, Italy). Numerical data of particles trajectories are available on iCFDdatabase (<http://mp0806.cineca.it/icfd.php>) kindly hosted by CINECA (Italy). More informations available upon request to the authors.

22. van Hinsberg M, ten Thije Boonkkamp J, Clercx H. An efficient, second order method for the approximation of the basset history force. *arXiv:10080833v1* 2010;.

References

1. Maxey MR, Riley JJ. Equation of motion for a small rigid sphere in a nonuniform flow. *Phys Fluids* 1983;**26**(4):883–889.
2. Gatignol R. The Faxén formulae for a rigid particle in an unsteady non-uniform Stokes flow. *J Mécanique Théorique et Appliquée* 1983;**1**(2):143–160.
3. Auton T, Hunt J, Prud’homme M. The force exerted on a body in inviscid unsteady non-uniform rotational flow. *J Fluid Mech* 1988;**197**:241–257.
4. Lovalenti PM, Brady JF. The hydrodynamic force on a rigid particle undergoing arbitrary time-dependent motion at small Reynolds number. *J Fluid Mech* 1993;**545**:561–605.
5. Michaelides EE. Review - the transient equation of motion for particles, bubbles, and droplets. *J Fluid Eng* 1997;**119**:233–247.
6. Loth E, Dorgan A. An equation of motion for particles of finite Reynolds number and size. *Env Fluid Mech* 2009;**9**:187–206.
7. Calzavarini E, Kerscher M, Lohse D, Toschi F. Dimensionality and morphology of particle and bubble clusters in turbulent flow. *J Fluid Mech* 2008;**607**:13–24.
8. Calzavarini E, Cencini M, Lohse D, Toschi F. Quantifying turbulence-induced segregation of inertial particles. *Phys Rev Lett* 2008;**101**:084504.
9. Volk R, Calzavarini E, Verhille G, Lohse D, Mordant N, Pinton JF, et al. Acceleration of heavy and light particles in turbulence: comparison between experiments and direct numerical simulations. *Physica D* 2008;**237**(14-17):2084–2089.
10. Calzavarini E, Volk R, Bourgoïn M, Lévêque E, Pinton JF, Toschi F. Acceleration statistics of finite-sized particles in turbulent flow: the role of Faxn forces. *J Fluid Mech* 2009;.
11. Qureshi NM, Bourgoïn M, Baudet C, Cartellier A, Gagne Y. Turbulent transport of material particles: An experimental study of finite size effects. *Phys Rev Lett* 2007;**99**(18):184502.
12. Brown RD, Warhaft Z, Voth GA. Acceleration statistics of neutrally buoyant spherical particles in intense turbulence. *Phys Rev Lett* 2009;**103**(19):194501.
13. Volk R, Calzavarini E, Lévêque E, Pinton J. Dynamics of inertial particles in a turbulent von Karman flow. *arXiv:10014943v1* 2010;.
14. Homann H, Bec J. Finite-size effects in the dynamics of neutrally buoyant particles in turbulent flow. *J Fluid Mech* 2010;**651**:81–91.
15. Schiller L, Naumann A. ber die grundlegenden berechnungen bei der schwärkeraufbereitung. *Vereines Deutscher Ingenieure* 1933;**77**:318–320.
16. Clift R, Grace JR, Weber ME. *Bubbles, Drops and Particles*. Academic Press (1978), Dover (2005); 1978.
17. Burton TM, Eaton JK. Fully resolved simulations of particle-turbulence interaction. *J Fluid Mech* 2005;**545**:67–111.
18. Elghobashi S, Truesdell GC. Direct simulation of particle dispersion in a decaying isotropic turbulence. *J Fluid Mech* 1992;**242**:655–700.
19. R. M, R.J. A. Flow past a sphere with an oscillation in the free-stream and unsteady drag at finite Reynolds number. *J Fluid Mech* 1992;**237**:323–341.
20. Mordant N, Pinton JF. Velocity measurements of a sphere settling in a fluid at rest. *Eur Phys J B* 2000;**18**:343–352.
21. Dorgan AJ, Loth E. Efficient calculation of the history force at finite Reynolds numbers. *Int J Multiphase Flow* 2007;**33**:833–848.